Experimental and Computational Analyses of the Anti-Alzheimer and Antidiabetic Effects of Flavonoid-rich Extract of Avocado Seeds (*Persea americana* Mill.)

Oluwafemi Adeleke Ojo[1,2,11*], Tobiloba Christiana Maduakolam-Aniobi [3], Gideon Ampoma Gyebi[4], Tenifayo Oluwatamilore Soyinka[1,2], Obianuju Favour Ejiogu[1,2], Adebola Busola Ojo[5] Mubarak Alruwaili[6], Naif H. Ali[7], Saud A. Alnaaim[8], Bshra A. Alsfouk[9], Gaber El-Saber Batiha[10]

[1] Good Health and Wellbeing Research Clusters (SDG 03) Bowen University, Iwo 232102, Nigeria.
[2] Phytomedicine, Molecular Toxicology, and Computational Biochemistry Research Group, Department of Biochemistry, Bowen University, Iwo 232102, Nigeria.
[3] Department of Biochemistry, Landmark University, Omu-Aran, Nigeria.
[4] Natural Products and Structural (Bio-Chem)-Informatics Research Laboratory (NpsBC-RI), Department of Biochemistry, Bingham University, Karu, Nigeria.
[5] Department of Environmental Management and Toxicology, University of Ilesa, Ilesa, Nigeria.
[6] Department of Internal Medicine, College of Medicine, Jouf University, Sakaka, Saudi Arabia
[7] Department of internal medicine, medical college, Najran university, Najran, SA.
[8] Clinical Neurosciences department, college of Medicine, King Faisal University, Hofuf- Saudi Arabia.
[9] Department of Pharmaceutical Sciences, College of Pharmacy, Princess Nourah bint Abdulrahman University, P.O. Box 84428, Riyadh 11671, Saudi Arabia
[10] Department of Pharmacology and Therapeutics, Faculty of Veterinary Medicine, Damanhour University, Damanhour, AlBeheira 22511, Egypt.
[11] Research Centre for Integrative Physiology and Pharmacology and Turku Center for Disease Modeling, Institute of Biomedicine, University of Turku, Turku, 20014, Finland.

*Corresponding authors: OAO: oluwafemiadeleke08@gmail.com

Abstract

Objectives: Our study examines the potential of flavonoid-rich extracts from avocado seeds (*Persea americana*) in combating Alzheimer's disease and diabetes.

Methods: The antidiabetic activity of the extracts was assessed via the inhibition of α-amylase and α-glucosidase enzymes. Additionally, their anti-Alzheimer properties were evaluated through their anti-cholinesterase activities against AChE, BChE, and monoamine oxidase (MAO). Molecular docking and dynamics simulations were conducted to identify potential flavonoid inhibitors for the enzymes α-amylase, α-glucosidase, AChE, BChE, and monoamine oxidase.

Key findings: Notably, the extracts exhibited significant inhibitory activity against AChE (IC_{50} = 38.105 ± 0.32 µg/mL) and BChE (IC_{50} = 72.542 ± 1.470 µg/mL). MAO suppression protected against Fe2+-mediated brain damage. Additionally, the flavonoid-rich extract of *P. americana* showed considerable inhibitory activity against α-amylase (IC_{50} = 608.516 ± 26.917 µg/mL) and α-glucosidase (IC_{50} = 790.570 ± 6.846 µg/mL) activities. HPLC-DAD profiling revealed the presence of gallic acid, caffeic acid, ferulic acid, rutin, p-coumaric acid, and quercetin. Molecular docking studies identified rutin, ferulic acid, and quercetin as the most promising ligands for the five protein targets investigated. Molecular simulations confirmed the stability of the protein–ligand complexes, as evidenced by favorable thermodynamic parameters.

Conclusions: Overall, our findings revealed that *P. americana* seed extracts have promising anti-Alzheimer's and antidiabetic effects.

Keywords: Pharmacology; Drug discovery; Medicinal plants; Noncommunicable diseases; Biocomputation

Introduction

Alzheimer's disease (AD) is a progressive neurodegenerative disorder characterized by cognitive decline, ultimately leading to various forms of dementia (Perluigi et al. 2024; Lekmine et al. 2024a). According to Tahami Monfared et al. (2022) and O'Neal (2024), approximately 1 in 9 individuals over 65 years of age are affected by AD, with women comprising two-thirds of the patient population. AD pathology is characterized primarily by the accumulation of toxic amyloid-beta (Aβ) plaques, neurofibrillary tangles of the tau protein, and neuroinflammation mediated by microglial activation. However, recent studies have emphasized the critical role of acetylcholinesterase (AChE), butyrylcholinesterase (BChE), and monoamine oxidases (MAOs) in the progression of AD and related dementias (Okpala et al. 2025, Ojo et al. 2024a). These enzymes are usually elevated in people with AD, leading to impaired cognitive function due to the inactivation of neurotransmitters such as acetylcholine, catecholamine and 5-hydroxytryptamine (Harilal et al. 2020; Walczak-Nowicka and Herbet 2021; Liu et al. 2022).

Emerging evidence suggests that diabetes mellitus significantly increases the risk of developing AD (Zhang et al. 2021a; Zhang et al. 2021b; Hamzé et al. 2022). According to a comprehensive review conducted by Zhang et al. (2021a), data from 24 longitudinal studies on diabetes indicate that people with diabetes have a relative risk of developing AD of 1.43% (CI= 1.25–1.62, 95%). Molecular studies on the crosstalk between AD and diabetes also suggest that AD pathogenesis is exacerbated when amyloid-beta, a protein implicated in AD, interacts with the islet amyloid peptide, a peptide implicated in diabetes (Zhang et al. 2021b; Hamzé et al. 2022). Studies have also shown that individuals with an abnormal glycemic index tend to have higher levels of phosphorylated tau proteins in their cerebrospinal fluid, which further implicates diabetes in the onset and progression of AD (Hobday and Parmar 2021; Rojas et al. 2021; Bellia et al. 2022). Since the brain is highly dependent on glucose metabolism, insulin resistance or insufficient insulin production can impair neuronal signaling, leading to deficits in memory formation, synaptic plasticity, and cognitive function (Sharma and Singh 2020; Blázquez et al. 2022). These findings suggest that therapeutic agents that target AChE, BChE and MAO and have antidiabetic effects could be effective in the management of AD and its associated dementias.

In silico studies play crucial roles in modern research by providing valuable insights into the potential biological effects of bioactive molecules from plant extracts. These computational approaches, including molecular docking, molecular dynamics simulations, and absorption, distribution, metabolism, excretion, and toxicity (ADMET) predictions (Lekmine et al. 2024b), allow researchers to analyze the interactions between plant-derived compounds and biological targets at the molecular level (Benslama et al., 2025). By simulating these interactions, in silico methods help identify promising bioactive molecules (Lekmine et al. 2025a), predict their binding affinities, and understand their mechanism of action before conducting extensive in vitro and in vivo experiments (Moussa et al., 2024). This not only accelerates the drug discovery process but also reduces costs, ethical concerns, and the need for excessive experimental testing. Furthermore, in silico studies aid in the optimization of lead compounds by assessing their pharmacokinetics and drug-likeness properties, thereby enhancing their therapeutic potential (Gherdaoui et al. 2024; Lekmine et al. 2025b). In the context of neurodegenerative diseases, metabolic disorders, and antimicrobial research, computational approaches provide a powerful tool for screening plant-derived compounds and identifying candidates for further biological validation (Ojo et al. 2022).

Plants serve as valuable sources of bioactive compounds that are widely utilized in traditional medicine and modern drug discovery. A single plant can be rich in lignans, flavonoids, tannins, polyphenols, triterpenes, sterols, and alkaloids, which endows the plant with immense medicinal properties. The different parts of a plant also contain varying concentrations and forms of these phytoconstituents, resulting in variations in the pharmacological activities of parts of the plant. *Persea americana* (*Mill*), commonly known as avocado, is one such plant, as a series of studies have explored the medicinal properties of different parts of the plant. The leaves of *P. americana* are rich in glycosides, alkaloids, tannins, saponins, flavonoids, and terpenoids (Boadi et al. 2015). The methanol extract from the leaves of *P. americana* also possesses strong antimicrobial properties against *Bacillus subtilis, Salmonella typhi, Streptococcus aureus, and Candida albicans* (Boadi et al. 2015). The fruits of *P. americana* are rich in vitamins, carotenoids, phenolic compounds and fatty acids

and possess anti-inflammatory, antioxidant and cardioprotective properties (Ochoa-Zarzosa et al. 2021).

Different extracts from the seeds of *P. americana* possess antidiabetic, antimicrobial, organ-protective, and hormone-regulatory properties (Ochoa-Zarzosa et al. 2021; Orabueze et al. 2021; Ojo et al. 2022a; Kupnik et al. 2023). In our previous study Ojo et al. (2022a), we explored the antidiabetic effect of the aqueous extract in an alloxan-induced rat model. Given the growing evidence of the molecular link between AD and diabetes, investigating the neuroprotective potential of known antidiabetic agents is essential. Hence, this research sought to evaluate the anti-Alzheimer's and antidiabetic properties of flavonoid-rich extracts from the seeds of *P. americana* via in vitro, *ex vivo* and in silico models.

Methods

Persea americana seed collection

The fruits of *P. americana* were collected from a local farm settlement in Ado-Ekiti metropolis, Ekiti State, after permission was obtained from the farm owner to collect the fruits of *P. americana*. The fruits were air-dried for several weeks and peeled to remove the seeds. The seeds were then chopped into shade-dried pieces before being pulverized into powder. The plant was authenticated and identified at the Forestry Research Institute of Nigeria (FRIN), and the voucher number was FHI 113162.

Preparation of flavonoid-rich extracts

Fifty grams of powdered *Persea americana* seeds were subjected to maceration (1:10) in 80% methanol for three days at room temperature to yield a crude methanolic extract (31.78 g). The mixture was stirred periodically. At the end of the extraction, the micelles were separated by filtration using cheesecloth. This crude extract was hydrolyzed by refluxing in 10% sulfuric acid at 100°C for 30 minutes (Ojo et al. 2024b). The resulting flavonoid aglycones were precipitated and dissolved in warm 95% ethanol, then filtered and diluted to 100 mL with 95% ethanol. The solution was concentrated under reduced pressure via a rotary evaporator. Flavonoids were extracted from the filtrate by precipitation with concentrated ammonium hydroxide, followed by washing with diluted ammonium hydroxide, with an extraction yield of 22.14 g (Ojo et al. 2024b).

Determination of the Enzyme Inhibitory Activities of Flavonoid-rich Extracts of *P. americana* Plants

Determination of α-amylase Inhibitory Activity

The method of Shai et al. (2010) was used to evaluate the α-amylase inhibitory property of flavonoid-rich extracts of *P. americana* seeds. Briefly, an aliquot of 5 µL of enzyme (Molychem, India) was made in cold 20 mM PBS (pH 6.7) and 6.7 mM NaCl. Thereafter, 250 µL of the enzyme was combined with the inhibitor acarbose or flavonoid-rich extract of *P. americana* (7.81–1000 µg/mL) at various concentrations, and the mixture was incubated at 37°C for 20 mins. A 0.5% (w/v) starch mixture was subsequently introduced, and the mixture was allowed to incubate for an additional 15 min at room temperature. Immediately after the mixture was incubated, DNS reagent was added, mixed and placed in a water bath at 100°C

for 10 mins. Finally, the absorbance was read at 540 nm. Acarbose was used as a standard. The experiment was performed in triplicate, and the percentage inhibition was determined.

The percentage inhibition was calculated as follows:

$$Percentage\ inhibition = \frac{Absorbance\ of\ control - Absorbance\ of\ sample}{Absorbance\ of\ control} x\ 100$$

Determination of the α-glucosidase Inhibitory Activity

The protocol was defined by Loukili et al. (2022). α-Glucosidase activity was measured at 400 nm spectrophotometrically by quantifying the release of p-nitrophenol from p-NPG. To evaluate α-glucosidase activity, 100 µL of 50 mM sucrose, 1000 µL of 50 mM phosphate buffer (pH 7.5), and 100 µL of α-glycosidase enzyme solution were prepared as the test solutions. Different solutions were added to this mixture, including a control (distilled water), positive control (acarbose), or flavonoid-rich extract of *P. americana* at varying concentrations (7.81–1000 µg/mL). The absorbance of the final solution was read at 500 nm. Acarbose served as the standard control. The percentage inhibition was then calculated.

The percentage inhibition was calculated as follows:

$$Percentage\ inhibition = \frac{Absorbance\ of\ control - Absorbance\ of\ sample}{Absorbance\ of\ control} x\ 100$$

Determination of the cholinesterase activity of flavonoid-rich extracts of *P. americana* seeds

The inhibitory effects of the flavonoid-rich extract of *P. americana* seeds on acetylcholinesterase (AChE) and butyrylcholinesterase (BChE) activities were determined via Ellman's method described by Perry et al. (2000). Briefly, 100 µL of the tissue samples mixed with varying concentrations of the flavonoid-rich extract were added to 50 µL of Ellman's reagent and 250 µL of 100 mM sodium phosphate buffer. The mixture was incubated for 20 min at 25°C, and 50 µL of 50 mM acetylcholine iodide was added. The absorbance was measured immediately at 412 nm at 3 min intervals for 15 min.

***Ex vivo* analysis**

Preparation of animals and organs

Healthy male Wistar rats, each weighing 150–200 g, were obtained from the Department of Biochemistry at Bowen University. After an overnight fast, the rats were euthanized with halothane. Their brains were then removed and homogenized in 1% Triton X-100 in 50 mM

phosphate buffer. The supernatants were collected in plain tubes for ex vivo research after homogenization was performed at 3,000 rpm and 40°C. The procedures followed the approved policies of the Bowen University Research Ethics Committee (approval number: BUI/BCH/2024/0004) and were reported in agreement with the ARRIVE guidelines.

***Ex vivo* induction of brain damage**

Ex vivo brain damage was induced via Fe^{2+}, following the methodology outlined by Erukainure et al. (2020) and Ojo et al. (2024b). In brief, 100 µL of 0.1 mM $FeSO_4$ was mixed with 200 µL of the tissue lysate containing varying concentrations (15–240 µg/mL) of the flavonoid-rich extract. The samples were then incubated for 30 min at 37°C before being used for biochemical evaluations. The reaction mixture containing only the tissue supernatant served as the normal control, whereas the mixture containing only the tissue supernatant and $FeSO_4$ served as the negative control.

Assessment of monoamine oxidase (MAO) activity

The monoamine oxidase (MAO) activity was evaluated following the protocol defined by Green and Haughton (1961). The orange–yellow color was quantified at a wavelength of 450 nm via a UV spectrophotometer and determined via the specified formula. Safinamide was used as the positive control for MAO activity.

%inhibition= Abscontrol− Abstest sample/Abscontrol ×100

HPLC–DAD analysis of flavonoid-rich extracts of *P. americana* seeds

An Agilent 1100-series HPLC system with a quaternary pump and UV-DAD detector equipped with a Zorbax Eclipse Plus C18 column (250 mm × 4.6 mm, 5 µm) was used. The oven temperature varied in the range of 0–55°C. Chromatographic separation was performed via a gradient elution method with H_2O:MeOH:THF, as described by Araujo-León et al. (2019). The mobile phase consisted of a gradient of (A) water containing 1% H_3PO and (B) methanol:tetrahydrofuran (80:20, v/v). The gradient program was as follows: 0–5 min, 90% A; 5–15 min, linear gradient to 50% A; 15–20 min, 50% A; 20–22 min, linear gradient to 90% A; 22–25 min, 90% A. The water contained 1% H_3PO, and the flow rate was 1.5 mL/min. A 20 µL sample was injected, and the column was purged and equilibrated for 10 minutes each.

Flavonoid standard compounds include rutin, quercetin, kaempferol, apigenin, gallic acid, caffeic acid, p-coumaric acid, and ferulic acid. Sample analysis took 40 minutes, and spectral data were collected. The column temperature was maintained at 25°C, and the detection wavelengths were set at 254 and 420 nm.

Molecular docking

Preparation of protein structure

Three-dimensional (3D) structures of protein–ligand complexes were retrieved from the Protein Data Bank (PDB) for human α-glucosidase complexed with acarbose (PDB ID: 3TOP), α-amylase complexed with acarbose (PDB ID: 1B2Y), butyrylcholinesterase (hBChE) complexed with decamethonium (PDB ID: 6EP4), monoamine oxidase B complexed with safinamide (PDB ID: 2V5Z), and acetylcholinesterase (hAChE) complexed with donepezil (PDB ID: 4EY7). Ligands and water molecules were removed from the downloaded crystal structures, and missing hydrogen atoms were added via GL-AutoDockTools (ADT, v1.5.6) (Fahmy et al. 2024, Ojo et al. 2025a; Ogunlakin et al. 2025).

Preparation of ligands

Structure data files (SDF) containing reference inhibitors (donepezil, decamethonium, acarbose, and safinamide) and HPLC-identified phytocompounds from *P. americana* seed extracts enriched with flavonoids were retrieved from the PuBChEm database. These compounds are already available in the database. These structures were then converted to the Protein Data Bank (PDB) chemical format via Open Babel software (v. 3.1.1). Nonpolar hydrogen atoms were merged with their bonded carbon atoms, whereas Gasteiger charges were assigned to polar hydrogen atoms. Finally, the prepared ligand molecules were converted to the dockable PDBQT format via AutoDock Tools (v. 4.2.6) (Benslama et al. 2023; Owumi et al. 2024). Prior to docking, the ligand structures were energy-minimized via Open Babel with the universal force field (UFF) and conjugate gradient descent algorithms.

Molecular Docking Validation

To evaluate the accuracy of our docking method, we compared the crystal structure of the extracted cocrystallized ligand with the predicted docking poses of the standard ligands (acarbose and donepezil) that had the lowest binding affinity in our initial docking. We used

Discovery Studio Visualizer to calculate the root-mean-square deviation (RMSD) between these structures.

Molecular docking of phytochemicals with targeted active sites

Molecular docking studies were conducted via the methods outlined in previous works (Ojo et al., 2022b; Okoli et al., 2022). Both standard inhibitors and HPLC constituents were docked into the active sites of five target proteins (Trott and Olson 2010). Before docking, we optimized the ligand structures via Open Babel and PyRx 0.8, employing the universal force field (UFF) and conjugate gradient descent algorithm (O'Boyle 2011). Table 1 provides the binding site coordinates for these target enzymes. We analyzed the molecular interactions between ligands and proteins via Discovery Studio Visualizer version 16, with default settings for additional parameters.

Molecular dynamics

To delve deeper into the dynamics of the top two phytochemical–protein complexes (4ey7 and 1b2y), we conducted 100 ns molecular dynamics simulations via GROMACS 2019.2 and the GROMOS96 43a1 force fields. Charmm-GUI was used to generate protein and ligand topology files (Lee et al. 2016; Lee et al. 2020). Other conditions of the simulations were as described in earlier reports (Gyebi et al., 2021; Ogunyemi et al., 2021, 2023). To maintain temperature and pressure, we employed velocity rescaling and the Parrinello–Rahman barostat, respectively (Owumi et al. 2024, Ojo et al. 2025b). The simulations were run with a 2 femtosec timestep via the Leap-Frog integrator, generating 1000 snapshots per system. From the MD trajectories, we calculated the RMSD, RMSF, ROG, SASA, and hydrogen bond interactions.

Calculation of the Binding Free Energy via the Molecular Mechanics Generalized Born Surface Area (MM-GBSA)

To quantify the binding affinities of the top two phytochemicals identified by docking, we employed the MM-GBSA protocol and associated decomposition analysis through the gmx MMPBSA package. This approach allowed us to calculate the binding energies of individual amino acid residues within 0.5 nm of the ligand (Miller III et al., 2012; Valdés-Tresanco et al., 2021). The methodology used here aligns with our previously published work (Gyebi et al., 2021; Ogunyemi et al., 2021).

Data analysis

Data analysis was performed via one-way ANOVA, and the results are expressed as the means ± standard deviations (n = 3). Statistical significance was determined at a p value < 0.05 via multiple comparisons. Graphical representations were generated via GraphPad Prism version 9.0.

Results

Experimental results

Effect of the flavonoid-rich extract of avocado seeds on diabetes indicators

Compared with the renowned antidiabetic drug acarbose, the flavonoid-rich extract of *P. americana (PA)* showed moderate inhibitory potential against α-amylase and α-glucosidase. As shown in Fig. 1A, the percentage inhibition of PA and acarbose increased in a dose-dependent manner. At 1000 µg/mL, PA inhibited amylase by 50%, whereas acarbose inhibited amylase by 90%. The concentrations of PA and acarbose required to inhibit amylase by 50% were 608.51 ± 26.91 µg/mL and 27.10 ± 0.27 µg/mL, respectively (Fig. 1B). At 1000 µg/mL, the percentages of α-glucosidase inhibited by PA and acarbose were 55% and 90%, respectively (Fig. 2A). As shown in Fig. 2B, the IC50 of PA (790.57 ± 6.84 µg/mL) was significantly lower than that of acarbose (17.39 ± 0.44 µg/mL). Although the inhibitory activity of PA against α-amylase and α-glucosidase is significantly lower than that of acarbose, the findings from this study indicate that the phytochemicals in PA could be explored as antidiabetic agents.

Effect of the flavonoid-rich extract of avocado seeds on brain indices

The anti-Alzheimer activity of the flavonoid-rich extract of *P. americana* was assessed on the basis of the ability of the extract to inhibit the activities of acetylcholinesterase (AChE), butyrylcholinesterase (BChE) and monoamine oxidase (MAO). As shown in Fig. 3A, the inhibitory activity of PA against AChE increased and compared favorably with that of galantamine. The concentrations of PA and galantamine required to inhibit 50% of AChE activity were 38.11 ± 0.33 µg/mL and 27.95 ± 0.122 µg/mL, respectively (Fig. 3B). Compared with that of galantamine, the inhibitory activity of PA against BChE also increased in a similar manner (Fig. 4A). However, the data presented in Fig. 4B show that the IC50 of PA (73.54 ± 1.47 µg/mL) was significantly greater than that of galantamine (23.13 ± 0.68 µg/mL). The data presented in Figure 5 show that PA (31.25–1000 µg/mL) significantly decreased iron-induced alterations in MAO levels in the brains of the exposed rats in a dose-dependent manner.

Phytochemicals in the flavonoid-rich extract of *P. americana*

HPLC-DAD screening of *P. americana* seeds revealed that the plant extracts contained gallic acid, caffeic acid, rutin, p-coumaric acid, ferulic acid and quercetin (Figure 6, Table 2).

Molecular docking results

Validation of the molecular docking

To evaluate our methodology, we superimposed the docked poses of reference compounds (donepezil and safinamide) with their lowest energy conformations onto the native ligands cocrystallized with the protein targets (4EY7 and 2V5Z) (Figure 1). We then calculated the root-mean-square deviation (RMSD) between the superimposed structures. The RDDs for donepezil and safinamide were 0.6211 and 0.7231 Å, respectively. These low RMSD values indicate that our docking protocol is suitable for predicting the binding poses of HPLC-identified phytochemicals.

Molecular docking of bioactive flavonoid compounds from flavonoid-rich extracts of *Persea americana* seeds against target proteins

After the validation protocol, with the same docking parameters, the HPLC-identified phytochemicals were docked to the active sites of the proteins. Table 3 presents the binding affinities of the HPLC-identified compounds docked to the five protein targets. On the basis of active site interactions, minimal binding affinities, and favorable binding poses, the two hit compounds for each target were selected for further analysis. The binding energies of these phytochemicals were ranked, and the top two compounds for each target exhibited binding energies comparable to those of standard inhibitors (Table 3). The cocrystallized reference compounds donepezil, decamethonium, acarbose, and safinamide for 4EY7, 6EP4, 1B2Y, 3TOP and 2V5Z were docked into the binding sites of the target proteins with binding affinity scores of -12.2, -5.4 -12.5, 14.2 and -11.1 kcal/mol, respectively. The binding affinity scores of the two hit compounds to the 4EY7, 6EP4, 1B2Y and 3TOP protein targets are -8.1, -9.8, -8.5 and -9.2 kcal/mol for quercetin and -9.4, -10.6, -8.9 and -8.8 kcal/mol for rutin, respectively, whereas those for 2V5Z are -7.5 kcal/mol for rutin and -7.3 kcal/mol for ferulic acid (Table 4). Among the top docked compounds, rutin demonstrated multiple top binding tendencies to all five protein targets, quercetin also demonstrated multiple top binding

tendencies to four protein targets, and ferulic acid was among the top two docked compounds to the 2V5Z protein targets.

Interactions of the two hit bioactive flavonoid compounds and standard compounds with the five protein targets

The interactions between the standard molecule and two hit bioactive flavonoids from the flavonoid-rich extract of *P. americana* seeds that were discovered via HPLC and had target protein binding site residues are displayed in Table 5. Most of the interactions between the ligand groups of the top docked phytochemicals and the enzyme residues were hydrophobic, with few H-bonds occurring below 3.40 Å.

Interactive analysis revealed that donepezil adopts a binding conformation in 4ey7 cells similar to that of the native ligand, extending into the long, narrow hydrophobic gorge. Quercetrin and rutin, the top-ranked phytochemicals for 4EY7, exhibited similar binding modes in the active site gorge (Table 5, Figure 8). The top-ranked phytochemicals (rutin and quercetin) established several hydrogen bonds with the catalytic amino acid residues involved in decamethonium binding (Figure 9). In the 1B2Y binding site, although acarbose extended into five subsites, the top phytochemicals (rutin and quercetin) occupied the -3 and -1 subsites (Figure 10). For 3TOP, the top phytochemicals (rutin and quercetin) adopted a binding mode similar to that of acarbose, interacting with corresponding amino acid residues (Figure 11). Unlike safinamide, which forms only one hydrogen bond with Gln206 and hydrophobic interactions, the top phytochemicals for MAO (ferulic acid and rutin) establish hydrogen bonds and hydrophobic interactions with amino acid residues (Figure 12).

Molecular dynamics simulation

Table 6 displays all of the parameter averages and standard deviations, whereas Figures 13–17 display the complex spectrum map. The RMSD plots for both systems (4EY7 and 1B2Y) revealed that equilibration occurred before 10 ns, with minimal fluctuations that were less than (±3) (Figure 13). The mean RMSD of the top docked compounds (rutin and quercetin) was greater than that of the reference compound acarbose. The mean RMSF values of the three 4EY7 systems were relatively consistent, and those of all the 1B2Y complex systems were comparable (Figure 14). The RoG graphs and SASA showed minimal fluctuations

throughout the simulation (Figures 15 and 16). The average number of hydrogen bonds formed in the entire molecule remained relatively stable during the experiment, with ligand-bound complexes exhibiting a similar number of hydrogen bonds (Figure 17).

Molecular mechanics generalized born surface area (MMGBSA) analysis

Through MMGBSA, we determined the binding free energies of the top two phytochemicals docked to 4ey7 and 1B2Y. Quercetrin exhibited the highest binding affinity for 4ey7, while rutin had the strongest binding affinity for 1B2Y. Notably, the binding free energies of the top phytochemicals docked to 4EY7 exceeded that of the reference compound, whereas only the binding free energy of rutin surpassed that of the reference inhibitor for 1B2Y. Quercetrin displayed a particularly low binding free energy of -0.68 ± 2.42. Table 7 provides a breakdown of the individual components contributing to the total binding free energy. Decomposition analysis revealed the specific amino acid residues involved in these energy contributions (Figures 18-19). Interestingly, the residues identified through static docking analysis were primarily responsible for the majority of the total binding free energy.

Discussion

The findings from this study showed that the flavonoid-rich extract of *P. americana* possesses moderate inhibitory activity against α-amylase and α-glucosidase, which is indicative of the antidiabetic properties of the plant. This finding is similar to the findings of Ojo et al. (2022a), who also suggested that an aqueous extract of *P. americana* could inhibit α-amylase and α-glucosidase. These two enzymes work synergistically to break down complex carbohydrates into glucose. However, overstimulation of these enzymes can lead to high blood sugar levels. By inhibiting these enzymes, *P. americana* can slow the breakdown of the complex into glucose, and the increase in blood glucose levels after meals is reduced. This is the mechanism of action of known antidiabetic agents such as acarbose, miglitol and voglibose (Hussain et al. 2023).

P. americana also showed dose-dependent inhibitory activity against AChE, BChE and MAO. These findings indicate that *P. americana* works by increasing the availability of neurotransmitters such as acetylcholine and catecholamine, which is the mechanism of action of the known anti-Alzheimer's drugs donepezil, rivastigmine and galantamine (Uddin

et al. 2021; Youdim 2022). A similar study published by Thu et al. (2019) reported that n-butanol extracts from the seeds of *P. americana* presented strong AChE inhibitory activity, which supports our findings that PA could be a promising agent for managing and treating AD.

The HPLC results revealed that *P. americana* contains gallic acid, caffeic acid, rutin, p-coumaric acid, ferulic acid and quercetin. These findings suggest that the anti-diabetic properties of PA are due to the presence of these compounds, as studies have reported the anti-diabetic properties of gallic acid (Rahimifard et al. 2020), rutin (Iqbal et al. 2024), quercetin (Shaikhomar and Bahattab 2021), caffeic acid (Xu et al. 2020), and ferulic acid (Qi et al. 2020). Gallic acid, caffeic acid and quercetin increase serum insulin levels and reduce diet-induced hyperglycemia (Rahimifard et al. 2020; Xu et al. 2020; Shaikhomar and Bahattab 2021). This finding suggests that the mechanism of action by which *P. americana* elicits its antidiabetic potential goes beyond the inhibition of α-amylase and α-glucosidase but transcends the stimulation of transcription factors involved in insulin sensitivity (Shaikhomar and Bahattab 2021; Ojo et al. 2022a).

Numerous reports have also revealed that gallic acid, rutin ferulic acid, and quercetin have anti-Alzheimer's disease effects (Szwajgier et al. 2020a; Orhan 2021; Li et al. 2023, Ojo et al. 2022). Like the findings presented in this study, (Orhan 2021) also identified quercetrin as a bifunctional molecule with antidiabetic and anticholinesterase activity. The findings from this study show that *P. americana* and its constituents could be used to treat diabetes and AD. The use of *P. americana* in the management of diabetes could also help reduce the risk of AD, as the compounds identified in *P. americana* are multifunctional and could help regulate the different pathways involved in the onset of AD.

In this study, identified bioactive flavonoids were docked against α-amylase and α-glucosidase via molecular docking, molecular dynamics and binding free energy calculations on the basis of MMGBSA. Rutin, quercetin, and ferulic acid were shown to be the top substances that docked to both enzymes.

Interestingly, most of the interactions between the ligand groups of the top docked phytochemicals and the enzyme residues were hydrophobic, with few H-bonds occurring below 3.40 Å.

For the 4EY7 interaction, the interactive analysis revealed that donepezil adopts a binding conformation in 4EY7 similar to that of the native ligand, extending into the long, narrow hydrophobic gorge. Quercetrin and rutin, the top-ranked phytochemicals for 4EY7, exhibited similar binding modes in the active site gorge. The top-ranked phytochemical rutin established several hydrogen bonds with catalytic amino acid residues (Leu76, Tyr72, Thr75, Asp74, Ser293, Gln291, Trp286, and Tyr341), whereas quercetin established hydrogen bonds with interacting amino acids (Tyr124, His287, Phe295, Trp286, Gln291, Leu289, Phe295, and Phe338). Furthermore, donepezil forms both hydrogen bonds (Phe295) and hydrophobic interactions (Leu289, Tyr72, Trp286, Tyr341, Tyr337, Phe338, Trp86, His447) at the active site of the protein.

In the 6EP4 binding site, decamethonium binding results in hydrophobic interactions at the sites with amino acid residues (His438, Trp82, and Asp70). Quercetrin forms both hydrogen bond interactions (Tyr124, His287, Phe295, Trp286, Gln291, Leu289, Phe295, and Phe338) and hydrophobic interactions (Tyr341, Trp286, and His287) at the active site. Rutin forms hydrogen bonds with the amino acids Leu76, Tyr72, Thr75, Asp74, Ser293, Gln291, Trp286, and Tyr341 at the target site and hydrophobic interactions with amino acid residues (Val294, Trp286, and Tyr341).

In the 1B2Y binding site, although acarbose extended into five subsites, the top phytochemicals (rutin and quercetin) occupied the -3 and -1 subsites. Acarbose forms hydrogen bonds with the interacting amino acid residues Trp59, Gln63, Tyr62, Thr163, GLy306, Thr163, His305, His299, Tyr62, Tyr151, His201, Lys200, Ile235, Arg195, Asp197, Lys200, Glu233, and Asp300 but only forms a single hydrophobic interaction with Trp59. Furthermore, quercetrin forms hydrogen bonds with amino acid residues at Tyr151, Thr163, Lys200, Ile235, Glu233, His299, Asp300, Trp59, Gly306, His305 and hydrophobic interactions at Lys200, Ile235, His201, Leu162, and Ala198. In addition, rutin forms hydrogen interactions with amino acids at Tyr151, Tyr62, Thr163, Gln63, Trp59, Asp356,

Val354, Arg195, His299, Asp300, Glu233, Asp197, Ala198 and hydrophobic interactions at Leu165, His101, Tyr62, Trp59, His305, and Asp356.

In 3TOP, the top lead compounds, rutin and quercetin, adopted a binding mode similar to that of acarbose, interacting with corresponding amino acid residues. The standard drug acarbose forms hydrogen bond interactions with amino acids at Asp1555, Arg1582, Asp1317, His1584, Trp1355, Thr1528, Gln1561, Lys1460, Asp1157, Met1421, Tyr1167, Arg1516, and Asp1526 and hydrophobic interactions at Tyr1251 and Phe1559. Furthermore, quercetrin forms hydrogen bonds with amino acid residues at Asp1279, His1584, Asp1420, Asp1526, Arg1510, Trp1369, Lys1460, and Asp1157 and hydrophobic interactions at Trp1355, Phe1559, and Tyr1251. In addition, rutin forms hydrogen interactions with amino acids at Lys1460, Asp1526, Tyr1167, Asp1157, Arg1510, Asp1420, Asp1279, Ile1280, Ile1587, and Thr1586 and hydrophobic interactions at Phe1559, Phe1560, Met1421, Tyr1251, and Trp1355.

Unlike safinamide, which forms only one hydrogen bond with Gln206 and hydrophobic interactions with Cys172, Ile316, Ile199, Tyr326, Tyr398, and Leu171. The lead compounds for monoamine oxidase (ferulic acid and rutin) established hydrogen bonds and hydrophobic interactions with amino acid residues. Ferulic acid forms hydrogen bonds with Ile199 Tyr326 Tyr398 Leu171 Tyr435 and hydrophobic interactions with Cys172, Tyr60, Phe343, and Tyr326. In addition, rutin forms hydrogen bonds with Tyr398, Gly434, Met436, Ser59, Tyr60, Tyr326, Gln206, Ile199, Leu164, Tyr435, Cys175, and Tyr188 and hydrophobic interactions with Leu171, Ile198, Ile199, and Tyr326.

Important residues that are connected to the inhibitory action of enzymes interact with phytochemicals. For example, the breaking of glycosidic linkages in polysaccharides has been found to be caused mostly by Asp197 of HPA. It has been documented that Asp197 plays a significant role as a catalytic nucleophile in hydrolytic processes for polymeric substrates such edible starch and that this residue interacts with known inhibitors (Zhang et al. 2009; Taha et al. 2019). Similar investigations have demonstrated interactions between the top docked phytochemicals and catalytic residues (Nawaz et al. 2020). The catalytic triad of Ser203, His447, and Glu334 clearly interacts with the best docked phytocompounds (Ordentlich et al. 1993).

The phytochemicals studied exhibited prominent π–π stacking interactions with aromatic residues, particularly those within the peripheral anionic site (P-site) located at the periphery of the gorge. This P-site plays a crucial role in substrate binding and allosteric interactions, facilitating substrate orientation and downward movement toward the catalytic serine (A-site) in AChE. Differences in the quantity of aromatic residues within the gorge between BChE and AChE contribute to differences in ligand binding specificity. Consequently, compounds that strongly interact with these catalytic residues, such as decamethonium, can inhibit enzyme catalysis (Darvesh et al., 2003; Colletier et al., 2006).

Importantly, recent studies have reported the in vitro cholinesterase inhibitory activities of quercetin and quercetin-3-O-rhamnoglucoside (rutin) (Khan et al. 2019; Szwajgier et al. 2020b; Iyiegbu and Enogieru 2024). Similarly, quercetrin, the glycosylated form (quercetrin and rutin) and rutin have been reported to have diabetic effects (Ghorbani 2017; Bule et al. 2019; Dhanya 2022; Maradesha et al. 2022).

Validation is essential for assessing the accuracy, precision, and reliability of a docking protocol (Gyebi et al., 2021). During the period of molecular dynamics, the stability of the complexes comprising the reference inhibitor (acarbose and donepezil) and representative proteins was examined via Tk console scripts. The trajectories obtained during the simulation were analyzed with respect to the number of H-bonds, RMSD, RMSF, RoG, and SASA (Ojo et al. 2024c). To determine the stability of the protein–ligand complexes, 100 ns molecular dynamics simulations were performed. Analysis of key thermodynamic metrics (RMSD, RMSF, RoG, SAS, and H-bond number) indicated that the complexes maintained structural integrity throughout the simulation. On the basis of our findings, the mean RMSD values revealed that for the two systems, 4EY7 and 1B2Y rutin and quercetrin presented minimal fluctuations. The 4EY7 systems presented consistent RMSF profiles, indicating comparable protein flexibility. RoG, SASA, and H-bond analyses revealed that the 4EY7 and 1B2Y complexes were stable throughout the simulation period.

Conclusion

Our results showed that *P. americana* possesses anti-Alzheimer's and antidiabetic properties by inhibiting enzymes linked to Alzheimer's disease (AChE, BChE, and MAO) and diabetes (α-amylase and α-glucosidase). In addition, computational analyses revealed that rutin, quercetin and ferulic acid were the top lead compounds against these target proteins. These findings imply that rutin, quercetin and ferulic acid are potential anti-Alzheimer's disease and antidiabetic drug agents. We recommend that in vivo experiments be performed to further evaluate our results.

Declaration

Ethical approval

The use of rats in this study was approved by the Bowen University Research Ethics Committee (BUREC) on March 21, 2024, with approval number BUI/BCH/2024/0004. All animal procedures adhered to the guidelines outlined by the Department of Biochemistry and the ARRIVE reporting standards.

Data availability statement

The experimental data that support the findings of this study are available in Mendeley with the identifier https://data.mendeley.com/datasets/b7m7ymrc22/1.

Author credit information

OAO conceived and designed the study. TCM-A, GAG, ABO, and OAO drafted the initial manuscript. TOS and OFE conducted the experiments. TCM-A, ABO, TOS, OFE, GAG, MA, NHA, SAA, BAA, GE-SB and OAO analyzed and interpreted the experimental data. OAO oversaw the experimental process. All the authors reviewed and approved the final manuscript.

Funding

This study did not receive any external funding whatsoever.

Conflict of interest

Not applicable

References

Araujo-León, J. A., Cantillo-Ciau, Z., Ruiz-Ciau, D. V., & Coral-Martínez, T. I. (2019). HPLC Profile and simultaneous quantitative analysis of tingenone and pristimerin in four Celastraceae species via HPLC-UV-DAD-MS. Revista Brasileira de Farmacognosia, 29, 171-176.

Bellia, C., Lombardo, M., Meloni, M., Della-Morte, D., Bellia, A. and Lauro, D. (2022). Diabetes and cognitive decline. *Advances in clinical chemistry*, 108, 37-71.

Benslama, O.; Lekmine, S.; Mansouri, N. Phytochemical Constituents of Astragalus Monspessulanus and Integrative Analysis for Its Antioxidant, Photoprotective, and Antityrosinase Activities: Experimental and Computational Investigation. *Eur J Integr Med* 2023, *60*, 102247.

Benslama, O.; Lekmine, S.; Moussa, H.; Tahraoui, H.; Ola, M.S.; Zhang, J.; Amrane, A. Silymarin as a Therapeutic Agent for Hepatocellular Carcinoma: A Multi-Approach Computational Study. *Metabolites* **2025**, *15*, 53.

Blázquez, E., Hurtado-Carneiro, V., LeBaut-Ayuso, Y., Velázquez, E., García-García, L., Gómez-Oliver, F., Ruiz-Albusac, J. M., Ávila, J. and Pozo, M. Á. (2022). Significance of brain glucose hypometabolism, altered insulin signal transduction, and insulin resistance in several neurological diseases. *Frontiers in Endocrinology*, 13, 873301.

Boadi, N. O., Saah, S. A., Mensah, J. K., Badu, M., Addai-Arhinand, S. and Mensah, M. B. (2015). Phytoconstituents, antimicrobial and antioxidant properties of the leaves of Persea americana Mill cultivated in Ghana. *Journal of Medicinal Plants Research*, 9 (36), 933-939.

Bule, M., Abdurahman, A., Nikfar, S., Abdollahi, M. and Amini, M. (2019). Antidiabetic effect of quercetrin: A systematic review and meta-analysis of animal studies. *Food and chemical toxicology*, 125, 494-502.

Colletier, J. P., Fournier, D., Greenblatt, H. M., Stojan, J., Sussman, J. L., Zaccai, G., Silman, I. and Weik, M. (2006). Structural insights into substrate traffic and inhibition in acetylcholinesterase. *The EMBO journal*, 25 (12), 2746-2756.

Darvesh, S., Hopkins, D. A. and Geula, C. (2003). Neurobiology of butyrylcholinesterase. *Nature Reviews Neuroscience*, 4 (2), 131-138.

Dhanya, R. (2022). Quercetrin for managing type 2 diabetes and its complications, an insight into multitarget therapy. *Biomedicine & Pharmacotherapy*, 146, 112560.

Erukainure, O.L.; Chukwuma, C.I.; Matsabisa, M.G.; Salau, V.F.; Koorbanally, N.A.; Islam, M.S. Buddleja saligna Willd (Loganiaceae) inhibits angiotensin-converting enzyme activity in oxidative cardiopathy with concomitant modulation of nucleotide hydrolyzing enzymatic activities and dysregulated lipid metabolic pathways. *Journal of Ethnopharmacology* 2020, *248*, 112358.

Fahmy, N.M.; Fayez, S.; Zengin, G.; Selvi, S.; Uba, A.I.; Mollica, A.; Bouyahya, A.; Ponniya, S.K.M.; Nilofar; Lekmine, S. Chemical Exploration of Different Extracts from Phytolacca Americana Leaves and Their Potential Utilization for Global Health Problems: In Silico and Network Pharmacology Validation. *J Biomol Struct Dyn* 2024, 1–21

Gherdaoui, D.; Yahoum, M.M.; Toumi, S.; Lekmine, S.; Lefnaoui, S.; Benslama, O.; Bouallouche, R.; Tahraoui, H.; Ola, M.S.; Ali, A. Elucidating Chiral Resolution of Aromatic Amino Acids Using Glycopeptide Selectors: A Combined Molecular Docking and Chromatographic Study. *Int J Mol Sci* **2024**, *25*, 9120.

Ghorbani, A. (2017). Mechanisms of antidiabetic effects of flavonoid rutin. *Biomedicine & Pharmacotherapy*, 96, 305-312.

Green, A. L.; Haughton, T. M. A. Colorimetric Method for the Estimation of Monoamine Oxidase. Biochemical Journal 1961, 78, 172–176.

Gyebi, G. A., Ogunyemi, O. M., Ibrahim, I. M., Afolabi, S. O. and Adebayo, J. O. (2021). Dual targeting of cytokine storm and viral replication in COVID-19 by plant-derived steroidal pregnanes: An in silico perspective. *Computers in biology and medicine*, 134, 104406.

Hamzé, R., Delangre, E., Tolu, S., Moreau, M., Janel, N., Bailbé, D. and Movassat, J. (2022). Type 2 diabetes mellitus and Alzheimer's disease: shared molecular mechanisms and potential common therapeutic targets. *International Journal of Molecular Sciences*, 23 (23), 15287.

Harilal, S., Kumar, R., Mathew, G. E., Jose, J., Uddin, M. S. and Mathew, B. (2020). Neurochemicals in nervous system and exploring the chemical make-up of human brain. *Principles of Neurochemistry: Fundamentals and Applications*, 19-39.

Hobday, A. L. and Parmar, M. S. (2021). The link between diabetes mellitus and tau hyperphosphorylation: implications for risk of Alzheimer's disease. *Cureus*, 13 (9).

Hussain, A., Latif, A., Rehmat, Z., Riaz, M., Jamil, N., Amir, M. and Asif, M. (2023). An updated review on anti-diabetic agents and their functions: a comparative study. *Advancements in Life Sciences*, 10 (3), 326-334.

Iqbal, A., Hafeez Kamran, S., Siddique, F., Ishtiaq, S., Hameed, M. and Manzoor, M. (2024). Modulatory effects of rutin and vitamin A on hyperglycemia induced glycation, oxidative stress and inflammation in high-fat-fructose diet animal model. *PLOS ONE*, 19 (5), e0303060.

Iyiegbu, M. E. and Enogieru, A. B. (2024). Antioxidant and anticholinesterase activity of rutin in aluminum chloride-exposed *Drosophila melanogaster*. *Comparative Clinical Pathology*, 1-8.

Khan, H., Ullah, H., Aschner, M., Cheang, W. S. and Akkol, E. K. (2019). Neuroprotective effects of quercetrin in Alzheimer's disease. *Biomolecules*, 10 (1), 59.

Kupnik, K., Primožič, M., Kokol, V., Knez, Ž. and Leitgeb, M. (2023). Enzymatic, Antioxidant, and Antimicrobial Activities of Bioactive Compounds from Avocado (Persea americana L.) Seeds. *Plants*, 12 (5), 1201.

Lee, J., Cheng, X., Swails, J. M., Yeom, M. S., Eastman, P. K., Lemkul, J. A., Wei, S., Buckner, J., Jeong, J. C. and Qi, Y. (2016). CHARMM-GUI input generator for NAMD, GROMACS, AMBER, OpenMM, and CHARMM/OpenMM simulations using the CHARMM36 additive force field. *Journal of chemical theory and computation*, 12 (1), 405-413.

Lee, J., Hitzenberger, M., Rieger, M., Kern, N. R., Zacharias, M. and Im, W. (2020). CHARMM-GUI supports the Amber force fields. *The Journal of chemical physics*, 153 (3), 035103.

Lekmine, S.; Benslama, O.; Tahraoui, H.; Ola, M.S.; Laouani, A.; Kadi, K.; Martín-García, A.I.; Ali, A. Anti-Cholinergic Effects of the Phenolic Extract from the Astragalus Crenatus Plant: A Computational and Network Pharmacology Study. Pharmaceuticals 2024a, 17, doi:10.3390/ph170303482**.**

Lekmine, S.; Benslama, O.; Kadi, K.; Ignacio Martín-García, A.; Shamsul Ola, M.; Abdullah Yilmaz, M.; Ali, A. Therapeutic Potential of Hyoscyamus Niger-Derived Compounds: Targeting Ovarian Cancer through Antioxidant Activity and EGFR Tyrosine Kinase Inhibition. *J King Saud Univ Sci* **2024b**, *36*, 103103, doi:https://doi.org/10.1016/j.jksus.2024.103103

Lekmine, S.; Benslama, O.; Bensalah, B.; Touzout, N.; Moussa, H.; Tahraoui, H.; Ola, M.S.; Hafsa, H.; Zhang, J.; Amrane, A. Bioactive Phenolics of Hyoscyamus Muticus L. Subsp. Falezlez: A Molecular and Biochemical Approach to Antioxidant and Urease Inhibitory Activities. *Int J Mol Sci* **2025a**, *26*, 370.

Lekmine, S.; Benslama, O.; Ola, M.S.; Touzout, N.; Moussa, H.; Tahraoui, H.; Hafsa, H.; Zhang, J.; Amrane, A. Preliminary Data on Silybum Marianum Metabolites: Comprehensive Characterization, Antioxidant, Antidiabetic, Antimicrobial Activities, LC–MS/MS Profiling, and Predicted ADMET Analysis. *Metabolites* **2025b**, *15*, 13.

Li, N., Yang, J., Wang, C., Wu, L. and Liu, Y. (2023). Screening bifunctional flavonoids of anti-cholinesterase and anti-glucosidase by in vitro and in silico studies: Quercetrin, kaempferol and myricetin. *Food Bioscience*, 51, 102312.

Liu, W., Wang, Y. and Youdim, M. B. (2022). A novel neuroprotective cholinesterase-monoamine oxidase inhibitor for treatment of dementia and depression in Parkinson's disease. *Aging Neur. Dis*, 2 (1).

Loukili, E.H.; Bouchal, B.; Bouhrim, M.; Abrigach, F.; Genva, M.; Kahina, Z.; Bnouham, M.; Bellaoui,
M.; Hammouti, B.; Addi, M.; et al. Chemical Composition, Antibacterial, Antifungal and Antidiabetic Activities of Ethanolic Extracts of Opuntia Dillenii Fruits Collected from Morocco. J. Food Qual. **2022**, 2022, 15.

Maradesha, T., Patil, S. M., Phanindra, B., Achar, R. R., Silina, E., Stupin, V. and Ramu, R. (2022). Multiprotein inhibitory effect of dietary polyphenol rutin from whole green jackfruit flour targeting different stages of diabetes mellitus: Defining a biocomputational stratagem. *Separations*, 9 (9), 262.

Miller III, B. R., McGee Jr, T. D., Swails, J. M., Homeyer, N., Gohlke, H. and Roitberg, A. E. (2012). MMPBSA. py: an efficient program for end-state free energy calculations. *Journal of chemical theory and computation*, 8 (9), 3314-3321.

Morris, G. M., Huey, R., Lindstrom, W., Sanner, M. F., Belew, R. K., Goodsell, D. S. and Olson, A. J. (2009). AutoDock4 and AutoDockTools4: Automated docking with selective receptor flexibility. *Journal of computational chemistry*, 30 (16), 2785-2791.

Moussa, H.; Dahmoune, F.; Lekmine, S.; Mameri, A.; Tahraoui, H.; Hamid, S.; Benzitoune, N.; Moula, N.; Zhang, J.; Amrane, A. Optimization of Ultrasound-Assisted Extraction of Bioactive Compounds from Carthamus Caeruleus L. Rhizome: Integrating Central Composite Design, Gaussian Process Regression, and Multi-Objective Gray Wolf Optimization Approaches. *Process Biochemistry* **2024**, *147*, 476–488.

Nawaz, M., Taha, M., Qureshi, F., Ullah, N., Selvaraj, M., Shahzad, S., Chigurupati, S., Waheed, A. and Almutairi, F. A. (2020). Structural elucidation, molecular docking, α-amylase and α-glucosidase inhibition studies of 5-amino-nicotinic acid derivatives. *BMC chemistry*, 14 (1), 1-11.

O'Boyle, N. (2011). Banck M. James CA Morley C. Vandermeersch T. Hutchison GR Open Babel: An open chemical toolbox. *J. Cheminf*, 3 (1), 33.

O'Neal, M. A. (2024). Women and the risk of Alzheimer's disease. *Frontiers in Global Women's Health*, 4, 1324522.

Ochoa-Zarzosa, A., Báez-Magaña, M., Guzmán-Rodríguez, J. J., Flores-Alvarez, L. J., Lara-Márquez, M., Zavala-Guerrero, B., Salgado-Garciglia, R., López-Gómez, R. and López-Meza, J. E. (2021). Bioactive molecules from native Mexican avocado fruit (Persea americana var. drymifolia): a review. *Plant Foods for Human Nutrition*, 76, 133-142.

Ogunlakin AD, Ojo OA, Gyebi GA, Akinwumi IA, Adebodun GO, Ayokunle DI, Ambali OA, Ayeni PO, Awosola OE, Babatunde DE, Akintunde EA, Ajayi-Odoko OA, Dahunsi OS, Sonibare MA. Elemental evaluation, nutritional analysis, GC–MS analysis and ameliorative effects of *Artocarpus communis* J.R.Forst. & G.Forst. seeds' phytoconstituents on metabolic syndrome via in silico approach. *Journal of Biomolecular Structure and Dynamics*, 2025; 43(4): 1981-2001

Ogunyemi, O. M., Gyebi, G. A., Ibrahim, I. M., Esan, A. M., Olaiya, C. O., Soliman, M. M. and Batiha, G. E.-S. (2023). Identification of promising multitargeting inhibitors of obesity from Vernonia amygdalina through computational analysis. *Molecular Diversity*, 27 (1), 1-25.

Ogunyemi, O. M., Gyebi, G. A., Ibrahim, I. M., Olaiya, C. O., Ocheje, J. O., Fabusiwa, M. M. and Adebayo, J. O. (2021). Dietary stigmastane-type saponins as promising dual-target directed inhibitors of SARS-CoV-2 proteases: a structure-based screening. *RSC advances*, 11 (53), 33380-33398.

Ojo, A.B.; Gyebi, G.; Alabi, O.; Iyobhebhe, M.; Nwonuma, CO.; Ojo, OA. *Syzygium aromaticum* (L.) Merr. & L.M.Perry mitigates iron-mediated oxidative brain injury by modulation of redox imbalance, cholinergic and purinergic dysfunctions, and glucose metabolizing enzymes activities. *Journal of Molecular Structure* **2022**, 1268C, 133675 doi: 10.1016/j.molstruc.2022.133675.

Ojo, O. A., Amanze, J. C., Oni, A. I., Grant, S., Iyobhebhe, M., Elebiyo, T. C., Rotimi, D., Asogwa, N. T., Oyinloye, B. E. and Ajiboye, B. O. Antidiabetic activity of avocado seeds (Persea americana Mill.) in diabetic rats via activation of PI3K/AKT signaling pathway. *Scientific reports*, 2022a;12 (1), 2919.

Ojo, O. A., Ogunlakin, A. D., Iyobhebhe, M., Olowosoke, C. B., Taiwo, O. A., Akinola, A., Fadiora, D., Odugbemi, A. I., Gyebi, G. A. and Nwonuma, C. O. Computer aided and experimental study of cinnamic acid analog for oxidative stress treatment: The therapeutic validations. *Informatics in Medicine Unlocked*, 2022b;35, 101137.

Ojo OA, Ajayi-Odoko OA, Gyebi GA, Ayokunle DI, Ogunlakin AD, Ezenabor EH, Olanrewaju AA, Agbeye OD, Ogunwale ET, Rotimi DE, Fouad D, Batiha GE-S, Adeyemi, OS. Network Pharmacology, Molecular Dynamics and In Vitro Assessments of Indigenous Herbal Formulations for Alzheimer's Therapy. *Life* 2024a, *14*, 1222. https://doi.org/10.3390/life14101222

Ojo OA, Gyebi GA, Ezenabor EH, Iyobhebhe M, Emmanuel DA, Adelowo OA, Olujinmi FE, Ogunwale TE, Babatunde DE, Ogunlakin AD, Ojo AB, Adeyemi OS. Exploring beetroot (*Beta vulgaris* L.) for diabetes mellitus and Alzheimer's disease dual therapy: in vitro and computational studies. *RSC Advances*, 2024b; 14, 19362 – 19380 DOI: 10.1039/d4ra03638g

Ojo OA, Adeyemo TR, Iyobhebhe M, Adams, MD, Asaleye RM, Evbuomwan IO, Abdurrahman, J, Maduakolam-Aniobi TC, Nwonuma, CO, Odesanmi OE, Ojo AB. *Beta vulgaris* L. beetroot protects against iron-induced liver injury by restoring antioxidant pathways and regulating cellular functions. *Scientific Reports* 2024c; 14, 25205. https://doi.org/10.1038/s41598-024-77503-6

Ojo OA, Ogunlakin AD, Gyebi GA, Ayokunle DI, Odugbemi AI, Babatunde DE, Akintunde EA, Ezea SC, Asogwa NT, Asaleye RM, Ojo AB. Profiling the antidiabetic potential of GC–MS compounds identified from the methanolic extract of *Spilanthes filicaulis*: experimental and computational insight. *Journal of Biomolecular Structure and Dynamics*, 2025a; 43(3): 1392-1413

Ojo OA, Adegboyega AE, Taiwo OA, Olowosoke CB, Johnson GI, Umedum NL, Onuh K, Adeduro MN, Nwobodo VO, Elekan AO, Alemika TE, Johnson TO. Lead optimization of *Allium sativum* L. compounds for PTP1B inhibition in diabetes treatment: in silico molecular docking and dynamics simulation. *Journal of Biomolecular studies and Dynamics* 2025b; 43(5); 2262-2276 DOI: 10.1080/07391102.2023.2294179

Okoli, B. J., Eltayb, W. A., Gyebi, G. A., Ghanam, A. R., Ladan, Z., Oguegbulu, J. C. and Abdalla, M. (2022). In silico study and excito-repellent activity of Vitex negundo L. Essential oil against Anopheles gambiae. *Applied Sciences*, 12 (15), 7500.

Okpala EO, Yeye OE, Ogunlakin AD, Eneogwe GO, Gyebi GA, Ojo OA, Odeja OO, Ibok MG, Ajiboye CO, Onocha PA, Lateef M, Ali MS. (2025). Derivatization and Anti-Butyrylcholinesterase Activity of Coumarinolignans: Experimental and Computational Approaches. *Chemistry Africa* (2025). https://doi.org/10.1007/s42250-025-01209-z.

Orabueze, I. C., Babalola, R., Azuonwu, O., Okoko, I.-I. and Asare, G. (2021). Evaluation of possible effects of Persea americana seeds on female reproductive hormonal and toxicity profile. *Journal of ethnopharmacology*, 273, 113870.

Ordentlich, A., Barak, D., Kronman, C., Flashner, Y., Leitner, M., Segall, Y., Ariel, N., Cohen, S., Velan, B. and Shafferman, A. (1993). Dissection of the human acetylcholinesterase active center determinants of substrate specificity. Identification of residues constituting the anionic site, the hydrophobic site, and the acyl pocket. *Journal of Biological Chemistry*, 268 (23), 17083-17095.

Orhan, I. E. (2021). Cholinesterase Inhibitory Potential of Quercetrin toward Alzheimer's Disease - A Promising Natural Molecule or Fashion of the Day? - A Narrowed Review. *Curr Neuropharmacol*, 19 (12), 2205-2213.

Owumi SE, Oluwawibe BJ, Chimezie J, Babalola JJ, Ogunyemi OM, Gyebi GA, Otunla MT, Altayyar A, Arunsi UO, Irozuru CE, Owoeye OO. An in vivo and in silico probing of the protective potential of betaine against sodium fluoride-induced neurotoxicity. BMC Pharmacol Toxicol. 2024;25(1):87.

Perluigi, M.; Di Domenico, F.; Butterfield, D.A. Oxidative Damage in Neurodegeneration: Roles in the Pathogenesis and Progression of Alzheimer Disease. *Physiol Rev* **2024**, *104*, 103–197.

Perry, N. S.; Houghton, P. J.; Theobald, A.; Jenner, P.; Perry, E. K. In-Vitro Inhibition of Human Erythrocyte Acetylcholinesterase by Salvia Lavandula Efolia Essential Oil and Constituent Terpenes. Journal Pharmaceutical 2000, 52, 895–902.

Qi, M.-y., Wang, X.-t., Xu, H.-l., Yang, Z.-l., Cheng, Y. and Zhou, B. (2020). Protective effect of ferulic acid on STZ-induced diabetic nephropathy in rats. *Food & function*, 11 (4), 3706-3718.

Rahimifard, M., Baeeri, M., Bahadar, H., Moini-Nodeh, S., Khalid, M., Haghi-Aminjan, H., Mohammadian, H. and Abdollahi, M. (2020). Therapeutic effects of gallic acid in regulating senescence and diabetes; an in vitro study. *Molecules*, 25 (24), 5875.

Rojas, M., Chávez-Castillo, M., Bautista, J., Ortega, Á., Nava, M., Salazar, J., Díaz-Camargo, E., Medina, O., Rojas-Quintero, J. and Bermúdez, V. (2021). Alzheimer's disease and type 2 diabetes mellitus: Pathophysiologic and pharmacotherapeutics links. *World Journal of Diabetes*, 12 (6), 745.

Shai, L., Masoko, P. & Mokgotho, M. (2010). Yeast alpha glucosidase inhibitory and antioxidant activities of six medicinal plants collected in Phalaborwa, South. *South African Journal of Botany*, 76, 465–470.

Shaikhomar, O. A. and Bahattab, O. S. (2021). Physiological effect of quercetrin as a natural flavonoid to be used as hypoglycemic agent in diabetes mellitus type II rats. *Saudi J Biomed Res*, 6 (1), 10-17.

Sharma, V. K. and Singh, T. G. (2020). Insulin resistance and bioenergetic manifestations: Targets and approAChEs in Alzheimer's disease. *Life Sciences*, 262, 118401.

Szwajgier, D., Borowiec, K. and Zapp, J. (2020a). Activity-guided isolation of cholinesterase inhibitors quercetrin, rutin and kaempferol from *Prunus persica* fruit. 75 (3-4), 87-96.

Szwajgier, D., Borowiec, K. and Zapp, J. (2020b). Activity-guided isolation of cholinesterase inhibitors quercetrin, rutin and kaempferol from *Prunus persica* fruit. *Zeitschrift Für Naturforschung C*, 75 (3-4), 87-96.

Taha, M., Noreen, T., Imran, S., Nawaz, F., Chigurupati, S., Selvaraj, M., Rahim, F., Hadiani Ismail, N., Kumar, A. and Mosaddik, A. (2019). Synthesis, α-amylase inhibition and molecular docking study of bisindolylmethane sulfonamide derivatives. *Medicinal Chemistry Research*, 28, 2010-2022.

Tahami Monfared, A. A., Byrnes, M. J., White, L. A. and Zhang, Q. (2022). Alzheimer's disease: epidemiology and clinical progression. *Neurology and therapy*, 11 (2), 553-569.

Thu, D. K., Thu Thuy, H., Thi Thanh Duyen, B., Thi Thanh Hang, L., Thi Trang, N., Son Nhat, B., Thi Quynh Hoa, T., Thi Ky Duyen, D. and Thanh Tung, B. (2019). Evaluating the Acetylcholinesterase Inhibitory and Antioxidant Activities of Persea Americana Extracts. *VNU Journal of Science: Medical and Pharmaceutical Sciences; Vol 35 No 1*.

Trott, O. and Olson, A. J. (2010). AutoDock Vina: improving the speed and accuracy of docking with a new scoring function, efficient optimization, and multithreading. *Journal of computational chemistry*, 31 (2), 455-461.

Uddin, M. S., Al Mamun, A., Kabir, M. T., Ashraf, G. M., Bin-Jumah, M. N. and Abdel-Daim, M. M. (2021). Multitarget drug candidates for multifactorial Alzheimer's disease: AChE and NMDAR as molecular targets. *Molecular Neurobiology*, 58, 281-303.

Valdés-Tresanco, M. S., Valdés-Tresanco, M. E., Valiente, P. A. and Moreno, E. (2021). gmx_MMPBSA: a new tool to perform end-state free energy calculations with GROMACS. *Journal of chemical theory and computation*, 17 (10), 6281-6291.

Walczak-Nowicka, Ł. J. and Herbet, M. (2021). Acetylcholinesterase inhibitors in the treatment of neurodegenerative diseases and the role of acetylcholinesterase in their pathogenesis. *International journal of molecular sciences*, 22 (17), 9290.

Xu, W., Luo, Q., Wen, X., Xiao, M. and Mei, Q. (2020). Antioxidant and anti-diabetic effects of caffeic acid in a rat model of diabetes. *Tropical Journal of Pharmaceutical Research*, 19 (6), 1227-1232.

Youdim, M. B. H. (2022). Site-activated multi target iron chelators with acetylcholinesterase (AChE) and monoamine oxidase (MAO) inhibitory activities for Alzheimer's disease therapy. *Journal of Neural Transmission*, 129 (5), 715-721.

Zhang, R., Li, C., Williams, L. K., Rempel, B. P., Brayer, G. D. and Withers, S. G. (2009). Directed "in situ" inhibitor elongation as a strategy to structurally characterize the covalent glycosyl-enzyme intermediate of human pancreatic α-amylase. *Biochemistry*, 48 (45), 10752-10764.

Zhang, X.-X., Tian, Y., Wang, Z.-T., Ma, Y.-H., Tan, L. and Yu, J.-T. (2021a). The epidemiology of Alzheimer's disease modifiable risk factors and prevention. *The journal of prevention of Alzheimer's disease*, 8, 313-321.

Zhang, Y., Tang, Y., Zhang, D., Liu, Y., He, J., Chang, Y. and Zheng, J. (2021b). Amyloid cross-seeding between Aβ and hIAPP in relation to the pathogenesis of Alzheimer and type 2 diabetes. *Chinese Journal of Chemical Engineering*, 30, 225-235.

Figure Legends

Figure 1: Inhibitory effect of a flavonoid-rich extract of *P. americana* on α-amylase

Legends: Data are presented as the means ± SDs (n = 3); $p < 0.0001$ according to t tests. *P. americana* seed; acarbose: standard drug

Figure 2: Inhibitory effect of the flavonoid-rich extract of *P. americana* on α-glucosidase

Legends: Data are presented as the means ± SDs (n = 3); $p < 0.0001$ according to t tests. *P. americana* seed; acarbose: standard drug

Figure 3: Inhibitory effect of the flavonoid-rich extract of *P. americana* on AChE

Legends: Data are presented as the means ± SDs (n = 3); $p < 0.0001$ according to t tests. *P. americana* seed; Galanthamine: standard drug

Figure 4: Inhibitory effect of the flavonoid-rich extract of *P. americana* on BChE

Legends: Data are presented as the means ± SDs (n = 3); $p < 0.0001$ according to t tests. *P. americana* seed; Galanthamine: standard drug

Figure 5: Inhibitory effect of the flavonoid-rich extract of *P. americana* on MAO

Legend: Data are presented as the means ± SDs (n = 3); $p < 0.0001$ according to ANOVA. ***P. americana*** seeds.

Figure 6: HPLC-DAD chromatogram identifying compounds in the flavonoid-rich extract of *P. americana*

Figure 7: Superimposition of the best docked conformer of the cocrytalized reference compound on the extracted conformation of (a) donepezil (b) safinamide. The green compounds represent the docked conformers, whereas the red and purple conformations represent the conformations extracted from 4EY7 and 2V5Z, respectively.

Figure 8: Top docked phytochemicals and reference inhibitor (donepezil) from the docking analysis of HPLC-identified phytochemicals from flavonoid-rich extracts of *P. americana* seeds that interact with amino acids in the active site of 4EY7. The ligands are displayed as sticks **(a)** Donepezil **(b)** Quercertrin (**c)** Rutin.

Figure 9: Top docked phytochemicals and reference inhibitor (decamethonium) from the docking analysis of HPLC-identified phytochemicals from flavonoid-rich extracts of *P. americana* seeds that interact with amino acids in the active site of 6EP4. (S) Surface representation of ligands in the binding sites of target proteins. The ligands are displayed as sticks **(a)** Decamethonium **(b)** Rutin (**c)** Quercetrin

Figure 10: Top docked phytochemicals and reference inhibitors (acarbose) from the docking analysis of HPLC-identified phytochemicals from flavonoid-rich extracts of *P. americana* seeds that interact with amino acids in the active site of 1B2Y. (S) Surface representation of ligands in the binding sites of target proteins. The ligands are displayed as sticks **(a)** Acarbose **(b)** Rutin (**c)** Quercetrin

Figure 11: Top docked phytochemicals and reference inhibitor (acarbose) from the docking analysis of HPLC-identified phytochemicals from flavonoid-rich extracts of *P. americana* seeds that interact with amino acids in the active site of 3TOP. (S) Surface representation of ligands in the binding sites of target proteins. The ligands are displayed as sticks **(a)** Acarbose **(b)** Rutin (**c)** Quercetrin

Figure 12: Top docked phytochemicals and reference inhibitor (safinamide) from the docking analysis of HPLC-identified phytochemicals from flavonoid-rich extracts of *P. americana* seeds that interact with amino acids in the active site of 2V5Z. (S) Surface representation of ligands in the binding sites of target proteins. The ligands are displayed as sticks **(a)** Safinamide **(b)** Ferulic acid (**c)** Rutin

Figure 13: Backbone-root mean square deviation (RMSD) plots of MD simulations of the top docked HPLC-identified phytochemicals (rutin and quercetin) and reference compounds complexed to (a) human acetylcholinesterase and (b) *human* α-amylase

Figure 14: Per residue root mean square fluctuation (RMSF) plots of the MD simulations of the top docked phytochemicals (rutin and quercetin) and reference compounds complexed to (a) *human* α-amylase and (b) human acetylcholinesterase

Figure 15: RoG plots of MD simulations of the top docked phytochemicals (rutin and quercetin) and reference compounds complexed to (a) human acetylcholinesterase (b) and *human* α-amylase

Figure 16: Surface accessible surface area (SASA) plots of MD simulations of the top docked phytochemicals (rutin and quercetin) and reference compounds complexed with (a) human acetylcholinesterase and (b) *human* α-amylase.

Figure 17: The number of hydrogen bonds in the complex systems of the top docked phytochemicals (rutin and quercetin) and reference compounds complexed to (a) human acetylcholinesterase and (b) *human* α-amylase

Figure 18: Molecular mechanics generalized band surface area (MM-GBSA) plot of the amino acid residues contributing to the total binding free energy of hAChE: (a) donepezil, (b) rutin, *and* (c) quercetin

Figure 19: Molecular mechanics generalized Born surface area (MM-GBSA) plot of the amino acid residues contributing to the total binding free energy of hAChE: (a) acarbose, (b) *rutin, and* (c) Quercetrin

Table 1. Dimensions of the binding site coordinates of the target enzymes

Dimensions	**3TOP** (Å)	**2V5Z**	**6EP4**	**1B2Y** (Å)	**4EY7**
center_x	-31.79	51.53	-20.23	18.87	-12.93
center_y	34.81	156.12	-40.64	6.13	-43.93
center_z	26.36	29.05	-23.74	47.10	27.45
Size x	22.08	25.0	23.07	22.08	23.38
Size y	25.28	25.81	23.67	23.46	20.10
Size z	22.08	22.84	22.31	20.473	19.81

Table 2: Bioactive principles identified in the flavonoid-rich extract of *P. americana* seeds

Compounds	**Retention time**
Gallic acid	2.822
p-coumaric acid	4.978
Ferulic acid	6.703
Caffeic acid	3.061
Rutin	4.262
Quercetrin	9.871

Table 3: The names and structures of the top two docked HPLC-identified phytochemicals from the flavonoid-rich extract of *P. americana* seeds against the five target proteins

S/No	Name	Structure
1	Ferulic acid	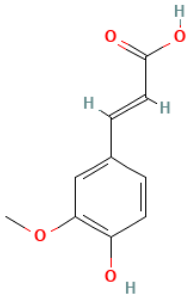
2	Quercitrin	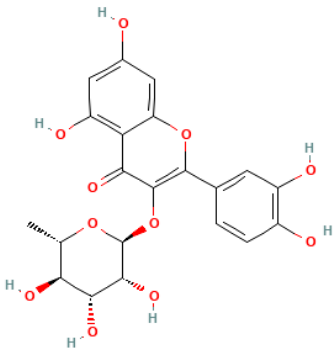
3	Rutin	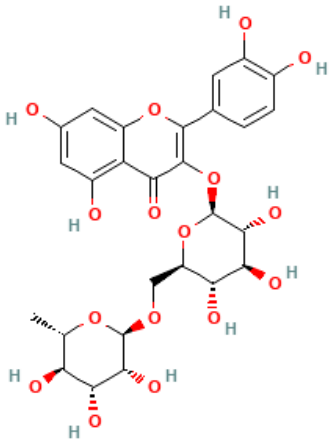

Table 4: Binding energies of the target compounds identified by HPLC from flavonoid-rich extracts of *P. americana* seeds

	Binding Affinity				
Ligand	3TOP	2V5Z	1B2Y	6EP4	4EY7
Donepezil (E=306.68)		-11.1		-9.6	-12.2
Safinamide (E=122.72)		-9.8			
Decamethonium (E=261.56)		-6.2		-5.4	-6.8
acarbose (E=372.76)	-14.2		-12.5		
p-coumaric_acid (E=90.82)	-7.3	-7	-6.2	-6.6	-7.6
Gallic acid (E=77.81)	-6.4	-6.3	-6.2	-6	-6.6
Ferulic acid (E=171.00)	-7	-7.3	-6.5	-6.8	-7.8
Caffeic_acid (E=98.70)	-6.9	-7.3	-6.6	-6.8	-7.7
Quercetrin (E=588.43)	-9.2	-6.8	-8.5	-9.8	-8.1
Rutin (E=751.29)	-8.8	-7.5	-8.9	-10.6	-9.4

Keywords: The binding energies of the standard and some compounds are related to the previously published work of Ojo et al. [2024]**.**

Table 5: Interaction of the phytochemicals selected from the docking analysis with the five target proteins

Compounds	Protein Targets	Hydrogen bonds	Hydrophobic Interaction
		Interacting residues	**Interacting residues**
Donepezil	4EY7	Phe295	Leu289 Tyr72 Trp286 Tyr341 Tyr337 Phe338 Trp86 His447
Quercetrin		Tyr124 His287 Phe295 Trp286 Gln291 Leu289 Phe295 Phe338	Tyr341 Trp286 His287
Rutin		Leu76 Tyr72 Thr75 Asp74 Ser293 Gln291 Trp286 Tyr341	Val294 Trp286 Tyr341
Decamethonium	6EP4		His438 Trp82 Asp70
Quercetrin		Tyr124 His287 Phe295 Trp286 Gln291 Leu289 Phe295 Phe338	Tyr341 Trp286 His287
Rutin		Leu76 Tyr72 Thr75 Asp74 Ser293 Gln291 Trp286 Tyr341	Val294 Trp286 Tyr341
Acarbose	1B2Y	Trp59 Gln63 Tyr62 Thr163 GLy306 Thr163 His305 His299 Tyr62 Tyr151 His201 Lys200 Ile235 Arg195 Asp197 Lys200 Glu233 Asp300	Trp59
Quercetrin		Tyr151 Thr163 Lys200 Ile235 Glu233 His299 Asp300 Trp59 Gly306 His305	Lys200 Ile235 His201 Leu162 Ala198
Rutin		Tyr151 Tyr62 Thr163 Gln63 Trp59 Asp356 Val354 Arg195 His299 Asp300 Glu233 Asp197 Ala198	Leu165 His101 Tyr62 Trp59 His305 Asp356
Acarbose	3TOP	Asp1555 Arg1582 Asp1317 His1584 Trp1355 Thr1528 Gln1561 Lys1460 Asp1157 Met1421 Tyr1167 Arg1516 Asp1526	Tyr1251 Phe1559
Quercetrin		Asp1279 His1584 Asp1420 Asp1526 Arg1510 Trp1369 Lys1460 Asp1157	Trp1355 Phe1559 Tyr1251
Rutin		Lys1460 Asp1526 Tyr1167 Asp1157 Arg1510 Asp1420 Asp1279 Ile1280 Ile1587 Thr1586	Phe1559 Phe1560 Met1421 Tyr1251 Trp1355
Safinamide	2V5Z	Gln206	Cys172 Ile316 Ile199 Tyr326 Tyr398 Leu171
Rutin		Tyr398 Gly434 Met436 Ser59 Tyr60 Tyr326 Gln206 Ile199 Leu164 Tyr435 Cys175 Tyr188	Leu171 Ile198 Ile199 Tyr326
Ferulic acid		Ile199 Tyr326 Tyr398 Leu171 Tyr435	Cys172 Tyr60 Phe343 Tyr326

Table 6: The means and standard deviations of the parameters analyzed from the MDS trajectories of the top docked compounds complexed with their respective targets.

	RMSD Mean (Å)	RMSF Mean(Å)	RoG Mean (Å)	SASA Mean (Å)	H-Bonds Mean (Å)
4EY7_ DONEPEZIL	1.69 ± 0.23	0.86 ± 0.70	23.10 ± 0.10	23046.95 ± 465.99	114.29 ± 9.23
4EY7_ RUTIN	1.72 ± 0.26	0.85± 0.29	23.41 ± 0.09	23121.45 ± 429.51	115.90 ± 9.81
4EY7_ QUERCETRIN	1.73 ± 0.12	0.86 ± 0.56	23.52 ± 0.09	23165.39 ± 473.26	115.25 ± 8.31
1B2Y_ ACARBOSE	1.53 ± 0.25	0.85 ± 0.53	23.33 ± 0.08	21387.142 ± 438.87	121.71 ± 9.37
1B2Y_ RUTIN	1.42 ± 0.25	0.81 ± 0.51	23.28 ± 0.09	20830.01 ± 425.35	126.27 ± 8.84
1B2Y_ QUERCETRIN	1.51 ± 0.23	0.84 ± 0.54	23.29 ± 0.11	21214.73 ± 459.58	124.41 ± 8.67

Table 7: Means and SDs of different energy components that determine the binding free energies of the top docked phytochemicals to target proteins

SYSTEM	EY7_ Donepezil	**4EY7_ Rutin**	**4EY7_ Quercetrin**	**1B2Y_ Acarbose**	**1B2Y_ Rutin**	**1B2Y_ Quercetrin**
$\Delta_{VDWAALS}$	-42.78 ± 3.08	-29.25 ± 3.17	-32.22 ± 3.23	-10.53 ± 8.67	-14.13 ± 2.86	-1.97 ± 3.96
Δ_{EEL}	-9.71 ± 11.53	-13.01 ± 6.50	-32.24 ± 11.24	-16.01 ± 20.79	-16.34 ± 12.0	-2.37 ± 5.75
Δ_{EGB}	38.59 ± 10.65	32.21 ± 6.2	55.16 ± 5.15	18.47 ± 19.76	21.94 ± 6.29	4.02 ± 7.63
Δ_{ESURF}	-5.99 ± 0.37	-3.09 ± 0.53	-5.08 ± 0.29	-2.25 ± 1.82	-2.71 ± 0.40	-0.36 ± 0.73
Δ_{GGAS}	-52.49 ± 12.24	-43.31 ± 1.34	-68.31 ± 5.15	-26.54 ± 27.77	-30.47 ± 11.8	-4.34 ± 8.97
Δ_{GSOLV}	32.6 ± 10.5	28.12 ± 2.09	50.18 ± 5.65	16.22 ± 18.05	19.24 ± 6.01	3.65 ± 6.95
Δ_{TOTAL}	-19.89 ± 3.61	-20.23 ± 6.18	-22.15 ± 4.13	-10.32 ± 10.61	-11.23 ± 7.05	-0.68 ± 2.42